How Do Hydrogen Bonds Break in Small Alcohol Oligomers?†

Ruomu Jiang and Edwin L. Sibert III*

Department of Chemistry and Theoretical Chemistry Institute, University of Wisconsin−Madison, Madison, Wisconsin 53706

Received: November 28, 2008; Revised Manuscript Received: January 16, 2009

Recent infrared pump−probe studies on alcohol oligomers in CCl_4 solution reveal that, following OH stretch excitation, ultrafast hydrogen bond (H-bond) breaking takes place on a time scale of 1 ps. To shed light on the mechanism of the H-bond breaking, we consider vibrational predissociation of the H-bonded methanol dimer. We construct a four-dimensional model for the dimer including the H-bond stretch, the donor OH stretch, the donor COH bend, and the OH rotation about the CO axis of the donor. Predissociation rates are calculated with Fermi's golden rule and close coupling approaches. Our results indicate that the predissociation leads to products with highly excited OH rotations. The predissociation rates strongly depend on the hydrogen bond strength. From our results, a simple nonadiabatic curve crossing picture for the predissociation process emerges, which provides a framework for future studies of solvent-assisted vibrational predissociation.

I. Introduction

Hydrogen-bonded (H-bonded) liquids like water and alcohols play vital roles in condensed-phase chemical processes. A molecular level understanding of the dynamics in these systems has been vigorously pursued by the physical chemistry community. The advance of ultrafast laser spectroscopy in the last two decades has enabled direct measurement of the vibrational dynamics in these systems with unprecedented time resolution. Combined with computer simulations, these efforts continue to shed light into the microscopic world of H-bonded liquids.

Much of the water and alcohol dynamics is dominated by the presence of H-bonds.[1] The OH stretch vibration is a sensitive probe for the H-bonding dynamics,[2,3] with its frequency dependent on the strength of the H-bonds in which it participates. It is well-known that the broad absorption peak in the OH stretch spectral region corresponds to an inhomogeneous distribution of H-bonding configurations in these liquids.[4] At equilibrium, the H-bonding configurations undergo rapid fluctuations and the H-bonds constantly break and reform. Nonequilibrium H-bond disruption after OH stretch excitation has recently been the subject of a series of experimental investigations.[5−17] The excited OH stretch energy, which typically exceeds the dissociation energy of an H-bond, could directly flow into the intermolecular H-bond stretch and subsequently break the H-bond. Such a process, known as vibrational predissociation, is a common feature among weakly bound gas-phase complexes.[18] In the case of liquid water, experiments reveal H-bond breaking on a subpicosecond time scale. While a predissociation mechanism has been suggested,[5] the H-bond breaking has been attributed to a sudden temperature jump following the vibrational energy relaxation (VER) of the OH stretch energy into the surrounding molecules.[7,8]

Compared to water, alcohol molecules such as methanol and ethanol serve as more benign model systems for studying H-bonding dynamics in the sense that on average they only participate in two H-bonds per molecule.[19] In the gas phase, H-bonded alcohol clusters are known to undergo vibrational predissociaton.[20] Predissociation spectra in the OH stretch region have helped determine the structure of various alcohol clusters.[21] The first experimental clue that this process might take place in the condensed phase came in 1989, when Graener et al.[9] carried out pump−probe experiments on ethanol oligomers in CCl_4 solution. Formation of ethanol molecules with broken H-bonds on a 5 ps time scale was observed following OH stretch excitation. The authors argued that the H-bond breaking could not have been due to the VER of the OH stretch, which at that time was believed to proceed on a longer time scale. Therefore it was proposed that the H-bond breaking was due to a direct predissociation of the oligomers. Later this process was revisited by several groups equipped with faster lasers; similar H-bond breaking events were reported. Laenen et al.[10] obtained 2 ps for the H-bond breaking time scale in the same system. In addition, evidence of near-resonant transfer of the OH stretch energy along the oligomer chain was suggested. Woutersen et al.[11] obtained a frequency-dependent lifetime ranging from 250 to 900 fs for the OH stretch excited state. Predissociation was invoked to account for the short population lifetime. Fast orientational relaxation was also reported, which supports the near-resonant energy transfer phenomenon proposed by Laenen et al.[10] The methanol oligomer system was also investigated by Laenen et al.[12] A frequency-dependent OH stretch excited state lifetime was reported to be between 450 and 600 fs in addition to the observed H-bond breaking. However, an assignment of the relaxation and H-bond breaking mechanism was not attempted. All the above work focused on the excitation of the internal OH groups that both donate and accept H-bonds. Fayer and co-workers[13−15] compared the different dynamics after excitation of the internal OD and the terminal OD, which does not donate a H-bond in deuterated methanol oligomers. Although the terminal OD was not expected to be strongly coupled to the H-bond, H-bond breaking with a 2 ps time constant was observed. This was referred to as an indirect breaking of the H-bonds and was explained as being preceded by a transfer of the initial excitation energy to the other methanol molecules within the excited oligomer. Following internal OD excitation, H-bond breaking with both 200 fs and 2 ps components was reported. The slower component of the H-bond breaking was

† Part of the "Robert Benny Gerber Festschrift".

* Address correspondence to this author.

10.1021/jp8104776 CCC: $40.75
Published on Web 03/06/2009

believed to be of the same origin as the indirect breaking in terminal OD excitation. The faster component was called a direct breaking of the H-bonds and could potentially be explained by predissociation.

The alcohol oligomers exhibit interesting H-bond breaking dynamics that clearly await more theoretical elucidation. Besides, a comparison of the dynamics in alcohol oligomers to that in water would provide a basis for our understanding of H-bonding in general. However, there are at least two major obstacles that prevent a straightforward simulation of the observed H-bond breaking. First, no theoretical framework is readily applicable to the predissociation problem in the condensed phase. Predissociation is in essence a quantum phenomenon and cannot be accurately treated with classical mechanics. Existing quantal treatments for predissociation only apply to isolated gas-phase complexes. The Landau−Teller theory,[22] which has been successful in treating condensed-phase VER problems, describes intermolecular modes, like the H-bond stretch, classically and thus is not suitable for treating the problem at hand. Second, the complexity involved in a system of alcohol oligomers in CCl_4 solvent is rather daunting from a computational perspective, since the cost of a quantal treatment increases exponentially with the number of degrees of freedom (DOFs) involved. A reduction of the experimental system to a certain idealized model system seems mandatory. To the best of our knowledge, there have only been two theoretical attempts to address the above experiments, with somewhat contradictory results. In 1993, Staib and Hynes[23] studied the predissociation of a gas-phase model system consisting of the OH stretch and the H-bond stretch. A time scale of 10 ps was obtained. Later, Staib[24] performed mixed quantum−classical molecular dynamics simulation of methanol dimer in CCl_4 solvent. By using a formula analogous to that of Landau−Teller, a time scale of 12 ns was obtained for the direct relaxation of the OH stretch into the classical H-bond stretch. It was thus concluded that the H-bond stretch alone as the accepting mode cannot produce a fast H-bond breaking.

While we focus on the predissociation pathway to the observed H-bond breaking, we must stress that an alternate route exists via the VER of the OH stretch. Kayano et al.[25] showed that in certain gas-phase H-bonded phenol complexes, intramolecular vibrational relaxation of the OH stretch precedes H-bond breaking. Moreover, although alcohol clusters undergo predissociation in the gas phase, the process does not necessarily carry over into the condensed phase. Shipman et al.[26] demostrated that the formic acid dimer dissociates after OH stretch excitation in the gas phase but does not do so in CCl_4 solution. Nevertheless, a quantitative simulation of the predissociation is needed to fully understand the experimental findings.

In this paper, we aim at investigating the detailed mechanism and efficiency of the alcohol oligomer predissociation process. A four-dimensional model system of the methanol dimer is constructed, including the H-bond stretch, the donor OH stretch, the donor OH torsion, and the donor COH bend. We believe this simple dimer model captures the essential physics of the intended process. The role of the CCl_4 solvent will be of secondary importance and will be examined in a future study. The gas-phase potential is calculated ab initio and is modified to reflect the H-bonding environment in the condensed phase. A vibrational self-consistent field (SCF) basis is employed to enable the Fermi's golden rule (FGR) calculation of the predissociation rates following OH stretch excitation. Predissociation rates are also obtained via close coupling (CC) calculations. Contrary to the mechanism suggested by Staib and Hynes,[23] an alternate mechanism for the predissociation emerges. Our current work also paves the road for future studies taking into account the solvent effect. The remainder of this article is laid out as follows. In Section II we discuss the theoretical background pertaining to the vibrational predissociation of weakly bound complexes. In Section III we describe our model system, focusing on the form of the kinetic energy operator and the calculation of the potential. Two different approaches to vibrational predissociation rates are outlined. After presenting the results in Section IV, we discuss the physical insight into the predissociation process in Section V. We give our conclusions in Section VI.

II. Theoretical Background

The vibrational predissociation of a broad range of gas-phase, weakly bound complexes, epitomized by the rare gas diatom complexes, have been subjected to extensive theoretical and experimental scrutiny. This process can be rigorously treated with scattering theory. Meanwhile, much physical insight can be gained by using a simple perturbative picture, the groundwork for which was laid down by Rosen.[27] On the basis of Rosen's original idea, Ewing[28] and Beswick and Jortner[29] pioneered the perturbative treatment of the van der Waals complex predissociation problem. The complex is initially excited into a zeroth-order quasibound state, corresponding to a certain vibrational excited state of the complex. The final states are zeroth-order continuum states corresponding to the two fragments flying apart with the initially excited fragment in certain lower vibrational states. The transition rate from the initial to the final states can be calculated according to FGR, which states that the rate is proportional to the square of the coupling matrix element between the initial and the final states. The de-excitation of the initial vibrational energy creates translational energy for the final continuum states and prompts the dissociation of the complex. In addition to translational energy, rotation of the fragments and other vibration of the fragments can be generated during the process, corresponding to different mechanisms of the predissociation.

For a rare gas diatom complex with weakly anisotropic interaction and small rotational constants for the diatom, such as $Ne \cdot I_2$, Beswick and Jortner showed that predissociation proceeds via a vibration to translation (V−T) mechanism.[29] Since the potential is weakly anisotropic, the angle of the diatom can be kept frozen, leaving only the diatom stretch and the dissociation coordinate. A quasibound state with a diatom stretch quantum number ν leads to products with a quantum number between $\nu - 1$ and 0, with $\nu - 1$ quanta being the dominant channel. Figure 1a schematically illustrates two effective potential surfaces, which differ by one diatom stretch quantum, as a function of the dissociation coordinate. The initial quasibound state is an eigenstate of the top surface called the bound surface and the final continuum state is an eigenstate of the bottom surface called the dissociative surface. Typically the weak interaction between the rare gas atom and the diatom results in similar shapes of the two surfaces. At the energy of the quasibound state, the classical turning point of the dissociative surface is radially shifted inward compared to that of the bound surface. This offset results in many oscillations of the continuum wave function in the region where the quasibound wave function has significant amplitude. This oscillation leads to relatively small overlap with the quasibound wave function and a generally long predissociation lifetime, exceeding nanoseconds, for this class of molecules.

For complexes with strong anisotropic interactions and large rotational constants for the excited fragment, the V−T mech-

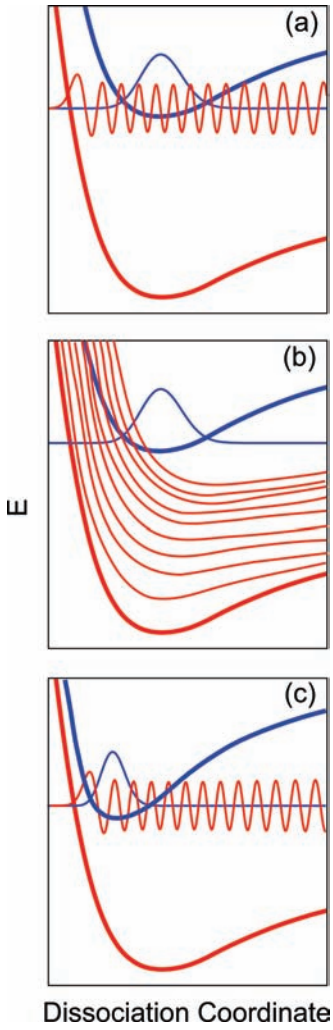

Figure 1. Effective potentials along the dissociation coordinate (a) for complexes that predissociate via V−T mechanism, (b) for complexes that predissocaite via V−TR mechanism, and (c) for the model considered by Staib et al.[23] In panels a and c, the top and bottom surfaces differ by one diatom stretch quantum number. In panel b, lower surfaces feature different amounts of intermolecular bend excitations.

anism predicts predissociation rates that are too slow. A vibration to translation and rotation (V−TR) mechanism turns out to be more efficient. Such examples include Ar·H_2,[30] Ar·HCl,[31] $(HF)_2$,[32] and Ne·C_2H_4.[33] The anisotropic interaction gives rise to a high-frequency intermolecular bending motion, which asymptotically corresponds to the rotation of the excited fragment. The role of this high-frequency intermolecular bend can be understood by looking at Figure 1b. The topmost surface is equivalent to the bound surface seen in Figure 1a. The bottom dissociative surfaces, together called a manifold, correspond to one less stretch quantum than the bound surface and different bend excitations. At the quasibound state energy, the classical turning points of the dissociative surfaces are radially shifted outward with increasing bend excitation compared to the surface with no bend excitation. This shift results in greater overlap between the continuum and the quasibound wave functions, which leads to a faster predissociation rate. Consequently the complex preferentially predissociates into highly excited bending channels, which asymptotically correspond to rotationally hot fragments.

The only calculation on gas-phase alcohol dimer predissociation has been carried out by Staib and Hynes.[23] Their model

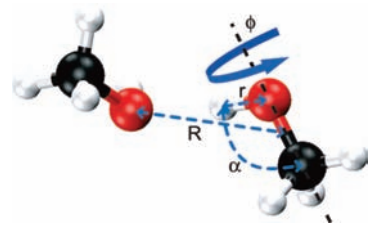

Figure 2. Structure of the methanol dimer and the coordinate definition of the four DOFs of our model.

TABLE 1: Calculated Normal Mode Frequencies (in cm^{-1})[a]

	monomer	donor	acceptor
OH stretch	3839	3674	3838
COH bend	1353	1416	1357
OH torsion	311	710	361
CO stretch	1047	1072	1041
CH_3 rock	1072	1116	1073

[a] Calculated at the B3LYP/6-31++G(d,p) level of theory and basis.

system includes the OH stretch and the H-bond stretch, which means predissociation can only occur via the V−T mechanism. An empirical Lippincott−Shroeder potential was employed that features strong coupling between the OH stretch and the H-bond stretch. The resulting effective potential surfaces are shown in Figure 1c. The bound surface is significantly shifted inward and also lowered compared to the bound surface of Figure 1a due to the aforementioned coupling. This creates favorable overlap between the continuum and quasibound wave functions, not seen in the gas phase van der Waals complexes. The calculated predissociation lifetime is on the order of 12 ps. It remains to be seen how these results will differ from an ab initio potential and what influence the other DOFs will have.

III. Methods

A. Methanol Dimer Model. In this section we describe a four-dimensional model that retains the essential physics of the predissociation process of the methanol dimer. The coordinate definitions are shown in Figure 2. The dissociation coordinate is the H-bond stretch. Intramolecular modes are selected based on their coupling to the dissociation coordinate. This coupling is reflected through frequency shifts upon forming a dimer. From the comparison in Table 1, the donor modes show stronger coupling to the H-bond stretch than their acceptor counterparts. Therefore the acceptor molecule is approximated as a structureless point mass located on the oxygen atom. The distance from this point to the center of mass of the donor molecule defines the H-bond stretch R. The donor OH stretch, whose coordinate r is the OH bond length, serves as the initially excited mode. We also include the OH torsion, whose coordinate ϕ is the dihedral angle defined by H−O−C−O atoms, and the COH bend, whose coordinate α is the COH bond angle. The OH torsion involves the rotation of the OH group around the CO axis and is analogous to the intermolecular bend and the azimuthal rotation that are vital in the V−RT mechanism of some van der Waals complexes. The COH bend is an important accepting mode in the VER of the OH stretch excited state in neat methanol[34,35] and can potentially exhibit a 1:2 stretch−bend Fermi resonance with the OH stretch. Other donor modes with smaller shifts, such as the CO stretch and CH_3 rock, are excluded at this stage but can be incorporated in future calculations. All other low-frequency interdimer modes are neglected as they are inefficient in transferring or absorbing energy during predissociation.

With the four DOFs that we explicitly include, our model can be thought of as an atom−triatom complex with the atom being the acceptor molecule and the triatomic molecule being the hydroxyl group plus the donor carbon atom. To obtain the Hamiltonian operator for this model, we begin with a generic form of the Hamiltonian in the center of mass frame for an atom−molecule scattering problem,

$$\hat{H} = -\frac{\hbar^2}{2\mu_R}\frac{\partial^2}{\partial R^2} + \frac{(\mathbf{J}-\mathbf{j})^2}{2\mu_R R^2} + \hat{H}^{\circ} + V'(R, r, \phi, \alpha) \quad (1)$$

where **J** and **j** are the angular momenta of the whole complex and of the molecule, respectively. The interaction potential V' describes the interaction between the atom and the molecule. The asymptotic Hamiltonian of the molecule $\hat{H}^{\circ}$, describes the isolated molecule and consists of the rotational kinetic energy operator and the intramolecular vibrational Hamiltonian of the molecule. The HOC pseudomolecule can perform azimuthal rotation about the CO axis or rotation within the plane defined by the CO axis and the atomic fragment. Since the HOC pseudomolecule can be approximated as a prolate top, the in-plane rotation of the molecule is slower than the azimuthal rotation, which is the OH torsion for our model. This allows the azimuthal and vibrational close-coupled rotational infinite order sudden (AVCC-IOS) approximation to be made,[33] where the in-plane rotation is factored out and the Hamiltonian is written for a fixed value of the in-plane rotational angle. That angle typically takes on the value of the potential minimum geometry of the complex. Here we make the further approximation of equating **j** with j_ϕ, which means the molecular fragment is only going to rotate around the CO axis. By restricting our attention to the case of **J** being zero, we force the whole complex to counter rotate about the CO axis to cancel the effect of the j_ϕ term. We then arrive at the Hamiltonian for our model,

$$\hat{H} = -\frac{\hbar^2}{2\mu_R}\frac{\partial^2}{\partial R^2} + \frac{j_\phi^2}{2\mu_{\text{eff}}R^2} + \hat{H}^{\circ} + V'(R, r, \phi, \alpha) \quad (2)$$

where $\mu_{\text{eff}}R^2$ is the moment of inertia of the whole complex rotating around the CO axis. The asymptotic Hamiltonian $\hat{H}^{\circ}$ takes on the form,

$$\hat{H}^{\circ} = \frac{j_\phi^2}{2I_\phi} - \frac{\hbar^2}{2\mu_r}\frac{\partial^2}{\partial r^2} - \frac{\hbar^2}{2\mu_\alpha}\frac{\partial^2}{\partial \alpha^2} - \frac{\hbar^2}{\mu_{r\alpha}}\frac{\partial^2}{\partial r \partial \alpha} + V^{\circ}(r, \phi, \alpha) \quad (3)$$

The effective masses μ_r, μ_α, and $\mu_{r\alpha}$ for the stretch and bend and the moment of inertia I_ϕ for the OH torsion are obtained by using the **G**-matrix formalism for an isolated methanol molecule.[36] The r dependences of μ_α and I_ϕ are included by Taylor series expansion of these terms about the potential minimum of the monomer to the third order. The remaining mass terms are treated as constants.

B. Potential Energy. When evaluating the asymptotic potential V°, the small amplitude nature of the OH stretch and COH bend warrants the usage of predetermined functional forms for the potential. To account for the anharmonicity of the OH stretch, a Morse potential is used,

$$V_r^{\circ} = D_e(1 - e^{-\beta(r-r_e)})^2 \quad (4)$$

with $\beta = (k_r/2D_e)^{1/2}$. The force constant k_r and the bond length r_e are functions of ϕ. The dissociation energy D_e of the OH bond is taken as a constant. Due to its comparatively weak anharmonicity, the potential along α is assumed to be harmonic,

$$V_\alpha^{\circ} = \frac{1}{2}k_\alpha(\alpha - \alpha_e)^2 \quad (5)$$

where k_α and α_e are similarly defined.

The potential along ϕ, which does not have a simple analytic form, is calculated ab initio for a methanol monomer at the B3LYP/6-31++G(d,p) level of theory and basis with Gaussian 98.[37] The OH torsion is the slowest DOF in the monomer. Therefore all other modes are allowed to adiabatically follow the OH torsion. Exploiting the C_{3v} symmetry of the torsional potential, the monomer is set to 5 different ϕ angles between 0° and 60°, and then allowed to relax to a minimum energy configuration while keeping the ϕ angle fixed. Subsequent calculations at the relaxed configurations produce the ϕ dependent energy V_e°, the OH bond length r_e, the COH bond angle α_e, as well as the force constants k_r and k_α. The asymptotic potential is then written as,

$$V^{\circ}(r, \alpha, \phi) = V_e^{\circ}(\phi) + V_r^{\circ}(r, \phi) + V_\alpha^{\circ}(\alpha, \phi) + V_{r\alpha}^{\circ}(r, \alpha, \phi) \quad (6)$$

where the additional $V_{r\alpha}^{\circ}$ term is the bilinear coupling between r and α also obtained from frequency calculations. Higher order potential couplings between r and α are neglected at this stage.

The evaluation of V' for the dimer is similar to that of V° for the monomer with the parameters now depending on both R and ϕ. However, since the H-bond stretch and the OH torsion are not the slowest DOFs in the dimer, all other DOFs cannot be allowed to adiabatically follow the H-bond and the OH torsion. The low-frequency interdimer modes that have been excluded from our model are not expected to undergo dramatic change during predissociation. Therefore, we freeze the interdimer orientation by fixing the two C−O−O angles and the C−O−O−C dihedral angle at their potential minimum values. Then at each of 20 values of R between 2.5 and 10 Å, all other DOFs are optimized. Corresponding to each R value, ϕ is then set to 24 different values between 0° and 360°. Assuming that the acceptor molecule is decoupled from the OH torsion of the donor molecule, at each value of ϕ, only the donor molecule is allowed to relax. Similar to the case of V_o, the ϕ and R dependent energy, bond length, bond angle, force constants, and bilinear coupling can be obtained from frequency calculations. The dimer potential can then be constructed in a similar fashion as eq 7, and the interaction potential by definition is the difference between the dimer potential and the asymptotic potential,

$$V'(R, r, \phi, \alpha) = V'_e(R, \phi) + V'_r(R, r, \phi) + V'_\alpha(R, \alpha, \phi) + V'_{r\alpha}(R, r, \alpha, \phi) - V^{\circ}(r, \alpha, \phi) \quad (7)$$

The potential V'_e is shown in Figure 3. The most noteworthy feature is the deep potential well around small R values due to the H-bonding interaction. As R increases, the H-bonding interaction diminishes causing the well depth to decrease and

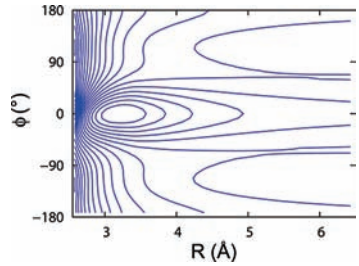

Figure 3. Two-dimensional potential energy surface V'_e plotted as a function of R and ϕ. The contour spacing is 300 cm^{-1}.

the feature corresponding to the three minima of the monomer torsional potential becomes more prominent.

To obtain numerical fits to the potentials, each term in V' and V^o is expanded as a sum of sine and cosine functions. For example, V'_e is written as,

$$V'_e(R,\phi) = \sum_{n=0}^{12} A_n(R)\cos(n\phi) + \sum_{m=1}^{12} B_m(R)\sin(m\phi) \quad (8)$$

The coefficients A_n and B_m are fitted to polynomials in R. The range of R is broken into a short-range piece (<4 Å) and a long-range piece (>4 Å). When fitting the long-range part, only terms that decay faster than R^{-6} are used to ensure the potential gradually goes to zero for large R. A switching function is employed to smoothly connect the two pieces.

C. Fermi's Golden Rule Approach. The basics of using FGR for calculating predissociation rates have been covered in the background section. Here we specify in detail the computational procedure and the choice of basis functions. To facilitate discussion we designate all other DOFs, other than the dissociation coordinate R, as **r**. The total Hamiltonian in eq 2 is separated into two terms,

$$\hat{H} = -\frac{\hat{\mathrm{h}}^2}{2\mu_R}\frac{\partial^2}{\partial R^2} + \hat{\mathrm{h}}(\mathbf{r};R) \quad (9)$$

where $\hat{h}(\mathbf{r};R)$ parametrically depends on R.

The first task is to find a set of vibrational basis functions for **r**. The basis functions are frequently chosen to be either eigenfunctions or approximate eigenfunctions of $\hat{h}(\mathbf{r};R)$, where some $\{\psi^i_n(\mathbf{r};R)\}$ correspond to initially excited states and the remaining $\{\psi^f_m(\mathbf{r};R)\}$ correspond to final predissociation product states. When expressed in a matrix representation of $\{\psi^i_n(\mathbf{r};R)\}$ and $\{\psi^f_m(\mathbf{r};R)\}$, $h(\mathbf{r};R)$ is divided into the diagonal blocks, $\mathbf{h}^{ii}(R)$ and $\mathbf{h}^{ff}(R)$, and the off-diagonal block $\mathbf{h}^{if}(R)$. The optimal choice of the basis functions ensures that the diagonal blocks are nearly diagonal. The diagonal elements $h^{ii}_{nn}(R)$ and $h^{ff}_{mm}(R)$ thus serve as the effective potential along the dissociation coordinate for quasibound states and continuum states with different **r** vibrational character. To solve for the quasibound state wave function Ψ^i_n and the continuum state wave function Ψ^f_m, they are written in product form as **r** basis functions times R dependent coefficients,

$$\Psi^i_n(\mathbf{r},R) = c^i_n(R)\psi^i_n(\mathbf{r};R) \quad (10)$$

$$\Psi^f_m(\mathbf{r},R) = c^f_m(R)\psi^f_m(\mathbf{r};R) \quad (11)$$

The validity of using one **r** basis function on the right-hand side relies on the condition that the diagonal blocks of the Hamiltonian are near diagonal. Otherwise the right-hand side is generally a linear combination of **r** basis functions. Plugging Ψ^i_n into the Schrödinger equation and integrating over the **r** space results in the eigenvalue problem,

$$\left[-\frac{\hbar^2}{2\mu_R}\frac{\partial^2}{\partial R^2} + h^{ii}_{nn}(R) - E^i_n\right]c^i_n(R) = 0 \quad (12)$$

which is solved to yield the quasibound state energy E^i_n and the corresponding wave function. The continuum state wave function is obtained by solving the following initial value problem for the E^f_m that is degenerate with a specific quasibound state,

$$\left[-\frac{\hbar^2}{2\mu_R}\frac{\partial^2}{\partial R^2} + h^{ff}_{mm}(R) - E^f_m\right]c^f_m(R) = 0 \quad (13)$$

The predissociation rate is computed according to the FGR as,

$$k_{nm} = \frac{2\pi}{\hbar}|\langle\Psi^i_n|h^{if}_{nm}|\Psi^f_m\rangle|^2\delta(E^i_n - E^f_m) \quad (14)$$

When choosing the basis representation $\{\psi^i_n(\mathbf{r};R)\}$ and $\{\psi^f_m(\mathbf{r};R)\}$, the commonly adopted diabatic representation, where the basis functions might be the eigenfunctions of the asymptotic Hamiltonian, assumes weak interaction potential.[31] This condition, however, does not hold for the potential shown in Figure 3. An alternative is the adiabatic representation where basis functions are the eigenfunctions of $\hat{h}(\mathbf{r};R)$ at each value of R. Applying this representation to our current problem allows basis functions with different stretch, torsion, and bend characters to mix thus producing avoided crossings between effective potential surfaces as demonstrated in Figure 4. At these crossings, large nonadiabatic couplings arise between these surfaces, which invalidates the presumption of eqs 11 and 12.

To avoid the large couplings associated with adiabatic representation, we adopt the SCF representation that is similar to the vibrational SCF representation pioneered by Gerber and Ratner,[38−40] but applied to a predissociation calculation. At every value of R, we iteratively solve for one-dimensional SCF wave functions for the **r** DOFs, the product of which forms the SCF basis. Compared to the diabatic representation, the SCF representation adapts to the interaction potential and thus overcomes the limitation to weak interaction. Meanwhile, since each component of the product basis retains well-defined OH stretch, COH bend, and torsional character, the representation is free of the avoided crossings that plague the adiabatic representation. This is demonstrated in Figure 4. We note that this SCF representation bears a resemblance to the electronic pesudodiabatic representation based on the idea of configuration uniformity.[41,42] The SCF wave functions parametrically depend on R and thus are subject to nonadiabatic couplings. However, since the SCF wave functions do not undergo abrupt changes, these couplings are assumed to be small enough that they can be ignored.

When performing the SCF calculation, 5 harmonic oscillator basis functions are used in both the r and α dimensions while 51 sine and cosine basis functions are used for the ϕ dimension.

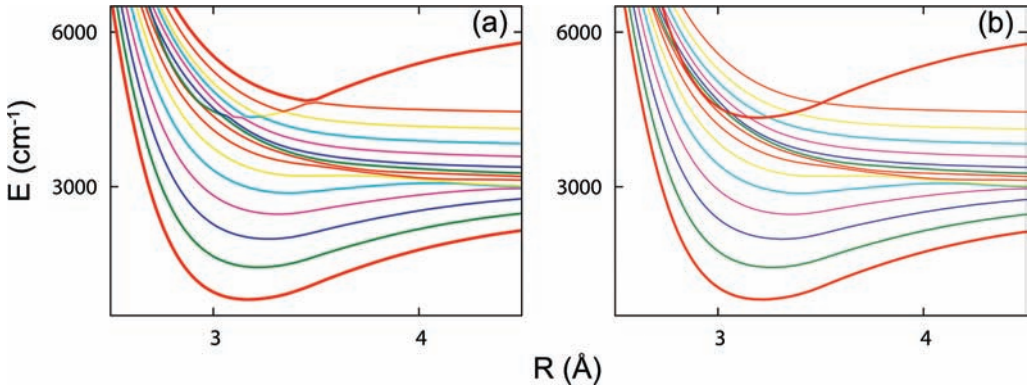

Figure 4. Effective potential surfaces plotted as functions of R. Both plots show the bound surface and the dissociative surfaces of the OH stretch and COH bend ground state manifold in (a) the adiabatic and (b) SCF representation.

Self-consistency is typically achieved within 3 cycles. When solving for the radial wave functions in eqs 13 and 14, matrix diagonalization is performed in a discrete variable representation (DVR)[43] for the quasibound state while the Numerov algorithm[44] is employed for the continuum state.

D. Close Coupling Approach. To evaluate the quality of the above approach, we also calculate predissociation rates with the CC method. This method has been successfully applied to predissociation problems and is more rigorous than the FGR method.[45] The predissociation process can be viewed as a half-collision, and the quasibound state corresponds to a resonance of the scattering wave function. The behavior of the scattering wave function in the vicinity of the resonant energy is analyzed, and the predissociation rate is related to the width of the resonance.

The computation procedure starts with finding the asymptotic channel functions, which are eigenfunctions of the asymptotic Hamiltonian H^o. The scattering wave function is expanded as a linear combination of the channel functions and substituted into the time-independent Schrödinger equation, which results in the close coupling equations. We adopt the **R**-matrix propagation method by Light et al.[46] to propagate these equations. The eigenphase sum, σ, of the scattering matrix is collected at the end of each propagation.[47] The propagation is repeated several times around the resonant energy, E_r. Finally the energy dependence of the eigenphase sum is fit to the Breit−Wigner formula,

$$\sigma(E) = \sigma_d(E) + \tan^{-1}\left\{\frac{\Gamma_r}{2[E_r - E]}\right\} \qquad (15)$$

and the resonant width Γ_r is extracted. The predissociation lifetime τ is inversely proportional to Γ_r via,

$$\tau = \frac{\hbar}{\Gamma_r} \qquad (16)$$

When obtaining the asymptotic channel functions, the same basis sets as in the FGR approach are used. For the **R**-matrix propagation calculation, about 30 basis functions are needed for each OH stretch and COH bend manifold. A typical calculation requires channels with up to two OH stretch quanta and three COH bend quanta, this yielding 360 total channels. To obtain an initial guess of the resonant energy, the full Hamiltonian in eq 2 is diagonalized in a product basis formed between the 360 channel functions and 15 DVR basis functions in the R dimension. Eigenvalues corresponding to the interested resonances are identified by analyzing the character of the eigenfunctions.

TABLE 2: Calculated and Experimental Vibrational Frequencies (in cm^{-1})

	molecule	stretch	bend	torsion
calcd	mono	3666	1253	208/242
exptl	mono	3686[a]	1340[b]	205/286[c]
calcd	dimer	3540	1356	604
exptl	dimer	3575[a]	1381[d]	613[e]
calcd	mono[f]	3666	1334	208/243
calcd	dimer[f]	3534	1396	606

[a] Reference 57. [b] Reference 58. [c] Reference 59. [d] Reference 34 for neat methanol. [e] Reference 60. [f] After adjustment of the COH bend quadratic force constant.

IV. Results

A. Variational Results. To gauge the performance of our methanol dimer model, the vibrational frequencies obtained by the variational calculation, which precedes the CC calculation, are compared with the experimental values in Table 2. The OH stretch frequencies are generally in good agreement with experimental values. The COH bend frequency in the monomer is underestimated while its blue shift in the dimer is overestimated by the calculation. The torsional frequency in the dimer agrees well with the experiment. In the monomer, the torsion splits into an A mode and an E mode due to the C_{3v} symmetry of the torsional potential. The calculated A−E splitting is much smaller than the experimental value.

The error in the COH bend frequencies originates from the local mode description of the bend employed in the model. A normal-mode analysis including all 30 vibrational DOFs of the methanol dimer reveals significant mixing between the COH bend, the CO stretch, and the methyl rock local modes. To remedy this problem, the dimer model can be expanded to incorporate the CO stretch and methyl rock. However, to keep the computational cost down, the monomer bend force constant is simply scaled and the interaction potential along the bend coordinate is decreased by a factor of 2 in order to better reproduce the experimental frequencies. The calculated frequencies after the adjustment are also listed in Table 2.

We now examine the discrepancy between the calculated and the experimental torsional frequencies. This difference is not due to the potential; the calculated torsional barrier, 423 cm^{-1}, is in reasonable agreement with the experimentally determined

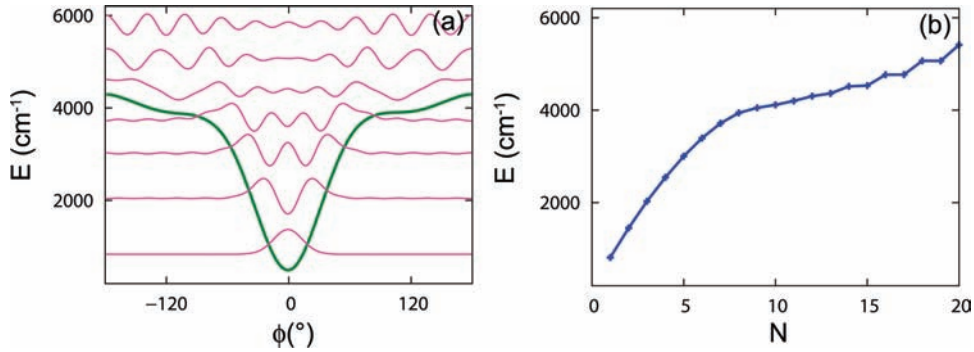

Figure 5. SCF torsional states at the potential minimum value of R: (a) SCF potential and selected torsional SCF wave functions χ_N plotted as functions of ϕ and (b) energies of the SCF torsional states plotted as functions of their quantum number N.

value.[48] The difference is due to the effective mass of the OH torsion, which is calculated for a motion only involving the OH group. This is based on the fact that in the dimer, the OH group is decoupled from the methyl group by forming the H-bond with the acceptor. However, in the monomer the torsion involves the counter-rotation of the OH and the methyl group. Thus, our model, while faithfully describing the torsion in the dimer, is inaccurate for describing the monomer torsion. When we switch to the true effective mass of the counter-rotation of the OH and the methyl group, the A−E splitting agrees much better with the experiment. Nevertheless, since predissociation happens in the dimer, treating the dimer correctly is more important than treating the monomer correctly. Consequently, our treatment for the torsion should be a good approximation as far as predissociation is concerned. Much greater computational complexity would be involved if both the OH and the methyl rotation were treated explicitly.

B. Calculations without the Bend. To isolate the effect of each mode on the predissociation lifetime, we first perform FGR calculations excluding the bend. This is achieved by setting potential and kinetic terms involving the bend to zero. As discussed in Section II, the shape of the effective potential surfaces along the dissociation coordinate has a profound impact on the predissociation lifetimes. The pivotal force in shaping the surfaces is first and foremost the H-bonding interaction potential along R, the form of which can be gleaned by cutting a slice through the potential in Figure 3 at a ϕ value of 0°. The OH stretch experiences a 120 cm^{-1} red-shift upon forming a dimer and has a minor impact on the OH excited manifold. The OH torsion, with its dramatic frequency shift, plays a major role in shaping the surfaces, especially the ones that correspond to excited torsional states. We now examine the behavior of the OH torsion in some detail. Around the potential minimum value of R, the SCF potential plotted in Figure 5a shows a steep well along the ϕ coordinate. Judging by the wave functions, the torsional states inside the well correspond to librational motion of the OH group in a narrow ϕ angular region and resemble harmonic oscillator states. At energies above the barrier of the well, the motion corresponds to rotation of the OH group about the CO axis. It is clear from Figure 5b that the torsional states inside the well are widely spaced while the states just above the barrier are densely packed. The same feature is also evident in Figure 4b. As R increases, the depth of the well along ϕ decreases, resulting in fewer torsional states inside the well. The energies of the states above the barrier thus decrease rapidly, leading to the negative slopes of the potential surfaces shown in Figure 4b.

The bound surface and selective dissociative surfaces together with their eigenfunctions are plotted in Figure 6. In Figure 6a,

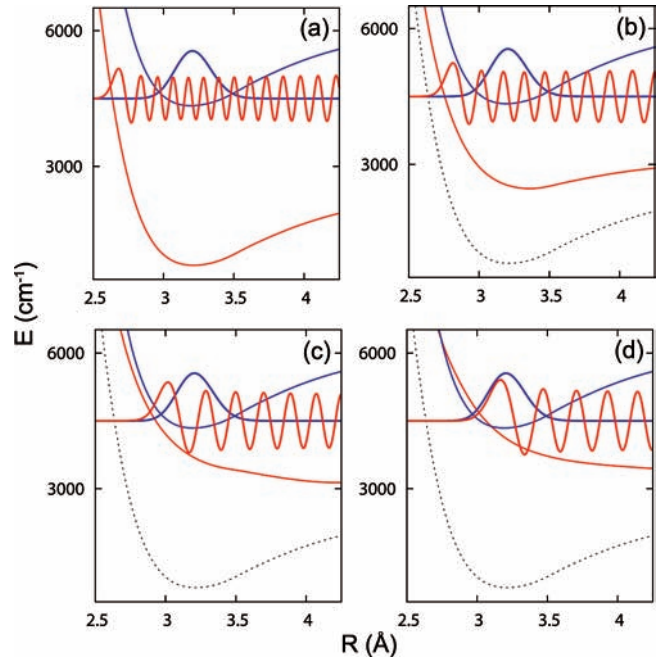

Figure 6. Bound and selective dissociative surfaces together with their wave functions plotted as functions of R. The dissociative surfaces (a−d) are respectively the 1st, 5th, 8th, and 12th surface with zero quantum in the OH stretch.

the dissociative surface is the lowest one among the OH stretch ground manifold with no torsional excitation. The corresponding predissociation process essentially obeys the V−T mechanism explained in the background section. The two surfaces strongly resemble those of Figure 1. As a result, the overlap between the quasibound and continuum wave functions is small, and predissociation on the time scale of 1 s is obtained. This picture is in striking contrast to that of Figure 1c; we will come back to this point later. Panels b−d of Figure 6 show a series of dissociative surfaces, which resemble those in Figure 1b, corresponding to increasing amount of torsional excitation. The diminished energy gap between the bound and the dissociative surfaces around the potential minimum value of R and the proximity between the classical turning points of the two surfaces both contribute to greater overlap between their wave functions. The negative slopes of a great number of dissociative surfaces help make these surfaces energetically accessible for the quasibound state.

Figure 7 shows the predissociation lifetimes into all dissociative surfaces that are energetically allowed. The H-bond stretch has a frequency of approximately 150 cm^{-1}, and at the temperature at which the experiments were carried out, its first few excited states are thermally populated. Thus we also

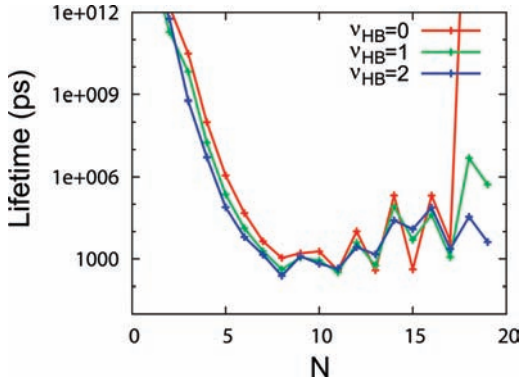

Figure 7. Predissociation time scales from three different quasibound states to all energetically allowed continuum states. *N* labels the continuum state on the *N*th dissociative surface.

TABLE 3: Predissociation Lifetimes (in ps)[a]

	$\nu_{HB} = 0$	$\nu_{HB} = 1$	$\nu_{HB} = 2$
FGR	97	88	86
CC	124	103	91
FGR tor ex[b]	38	27	23
CC tor ex[b]	56	41	38

[a] Calculated with both FGR and CC approaches excluding the COH bend. [b] For initial states with one quantum of torsional excitation.

consider the first two H-bond stretch excited quasibound states. For all three quasibound states, the lifetime is long for low-lying surfaces and gradually shortens as the *N* number increases. The fastest predissociation occurs between surface 8 and 15, where the lifetime shows some oscillation. From Figure 5, it is clear that these surfaces all correspond to rotation of the OH group over the barrier at the potential minimum region of *R*. Furthermore Figure 4b shows that these surfaces all have near or actual crossings with the bound surface.

Total predissociation rates obtained from the FGR approach are summarized and compared to those from the CC approach in Table 3. The agreement between the two methods is generally good. The lifetimes of all three quasibound states are on the order of 100 ps. Both methods show decreasing lifetimes as the number of quanta in H-bond stretch increases, although the change is more dramatic in the close coupling case.

These results suggest that the H-bond stretch cannot efficiently take up all the energy from the OH stretch so the V−T route to predissociation is extremely slow. However, the OH torsion can facilitate the predissociation via a process similar to the V−RT mechanism. In addition, when considering the quasibound states with one quantum of torsional excitation, the predissociation lifetimes are shortened by a factor of 2−3 as shown in Table 3 compared to the quasibound states without torsional excitation. This result further substantiates the idea that the OH torsion facilitates predissociation. CC calculations with just the OH stretch and the H-bond stretch were also performed. As expected, the resonance is too narrow to be detected.

C. Calculations with the Bend. In the methanol dimer, because the COH bend experiences a blue-shift and the OH stretch experiences a red-shift compared to the monomer, the OH stretch can potentially exhibit a 1:2 Fermi resonance with the bend. Similar resonance has been found to result in an accelerated intramolecular relaxation of neat methanol after OH stretch excitation.[34,35] Predissociation lifetimes from calculations including the COH bend are listed in Table 4. The inclusion of the bend does not alter the lifetimes considerably.

TABLE 4: Predissociation Lifetimes (in ps)[a]

	$\nu_{HB} = 0$	$\nu_{HB} = 1$	$\nu_{HB} = 2$
FGR	106	94	89
CC	98	81	76

[a] Calculated with both FGR and CC approaches including the COH bend.

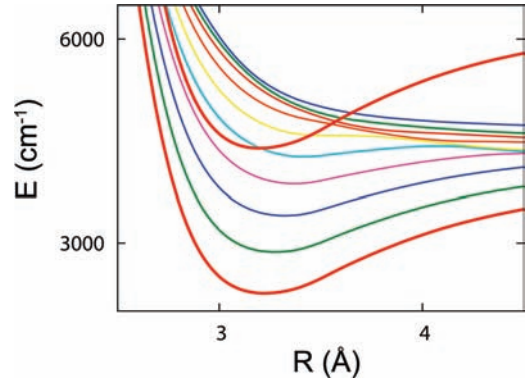

Figure 8. Bound and dissociative surfaces on the OH stretch ground and the COH bend first excited state manifold plotted as functions of *R*.

To understand this result, we first consider the additional predissociation pathways brought about by including the bend. Despite the possible Fermi resonance, the OH stretch does not contain enough energy to simultaneously excite two quanta in the COH bend and break the H-bond. It can, however, excite one quantum of bend while breaking the H-bond. Figure 8 shows the bound surface and the dissociative surfaces of the COH bend excited state manifold. When compared to those in Figure 4b, these dissociative surfaces are shifted up toward the bound surface by the energy of a quantum of COH bend. Therefore, far fewer dissociative surfaces have near or actual crossings with the bound surface. As a result, predissociation into the COH bend excited manifold is not very efficient. Alternatively, just as in the calculations excluding the bend, the quasibound state can predissociate into continuum states of the OH stretch and COH bend ground manifold. The COH bend, with a frequency shift of 60 cm^{-1}, does not significantly influence this pathway.

D. Calculation with Scaled Potential. Due to the cooperative nature of the H-bonding network, alcohol oligomers are connected by stronger H-bonds than that between the gas-phase methanol dimer. This can be seen from the much greater red-shift of the OH stretch for the oligomers, around 300 cm^{-1}, than that for the gas-phase dimer, only 120 cm^{-1}. Evidently, it is important to understand how the predissociation lifetime depends on the strength of the H-bond. To this end, we simply scale the interaction potential along the OH stretch by different factors to account for different H-bond strength. The red-shift of the OH stretch changes linearly with the scaling factor. The zeroth-order interaction potential along *R* and ϕ as seen in Figure 3 is not scaled. The COH bend is excluded from this calculation.

The lifetimes calculated from both FGR and CC approaches when plotted against the OH stretch red-shift in Figure 9 show an almost exponential dependence on the red-shift. One might expect that the lifetimes should quadratically depend on the scaling factor, given the square relationship between the coupling matrix element and the rate in the FGR formula. However, the scaling also changes the shape of the bound and dissociative surfaces and thus the overlap of their eigenfunctions. For a strongly hydrogen bonded dimer with a red-shift over 300^{-1}, predissociation lifetimes are on the order of a few

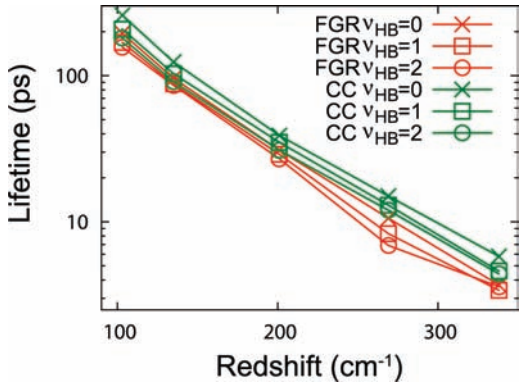

Figure 9. Predissociation lifetimes plotted as functions of the OH stretch red shift in log scale for three different quasibound states, calculated with both FGR and CC approaches.

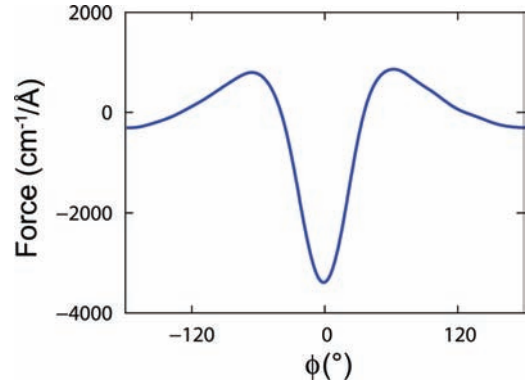

Figure 10. Linear force along the OH stretch plotted as a function of ϕ at the potential minimum value of R.

picoseconds. It is important to note that even though the predissociation lifetimes are dramatically shortened, the mechanism is unchanged. When examining predissociation rates into individual dissociative surfaces, the general pattern seen in Figure 7 still holds. Even with a relatively strong H-bond, the V−T mechanism remains inefficient.

V. Discussion

The FGR and CC calculations suggest that the direct OH stretch vibration to H-bond stretch translation transfer is inefficient. This conclusion is in disagreement with that of Staib and Hynes.[23] The discrepancy stems from the qualitative difference between their empirical Lippincott−Shroeder potential and our ab initio potential. The difference is illustrated by the striking dissimilarity between the bound potential surface in Figure 4b and that in Figure 1c. To clarify this point, we focus on an important quantity, the derivative of the OH bond length r_e with respect to the H-bond length. This quantity, which is a measure of the coupling between the OH stretch and the H-bond stretch, is about 200 times larger in the work by Staib and Hynes than in our ab initio potential. Even when we scale the interaction potential to account for different H-bonding strength, this quantity is scaled by no more than a factor of 2.5. We conclude that the potential employed by Staib and Hynes overestimates the coupling between the OH stretch and the H-bond stretch, giving rise to an overestimated V−T predissociation rate.

Our calculation suggests that the quasibound state with torsional ground state character is coupled to continuum states with high torsional excitation. This might seem surprising considering the torsional excited state SCF wave functions oscillate rapidly around the region where the torsional ground state SCF wave function has significant amplitude, as evident in Figure 5. To understand the origin of this strong coupling, we can temporarily assume the OH stretch to be harmonic and ignore the bend. The quasibound and the continuum states differ by one quantum in the OH stretch, thus the dominant coupling between them should be the linear force along r. This force, which still depends on both R and ϕ, is plotted along ϕ for the potential minimum value of R in Figure 10. One sees a strong ϕ dependence of the force. For ϕ values around 0°, the large negative force implies an elongated OH bond of the dimer compared to that of the monomer due to H-bonding interaction. For ϕ values around 180°, the small force implies an OH bond length similar to that of the monomer due to a broken H-bond. Clearly the ϕ dependence of the force originates from the anisotropy of the H-bonding interaction. This force leads to a relatively large coupling matrix element when averaged over the SCF basis functions of the quasibound and continuum states and enables the predissociation to proceed efficiently.

The following physical picture emerges for the predissociation process. When the initial vibrational energy leaves the OH stretch, it transfers into the OH torsion. The donor OH group is then propelled to spin around the CO axis. Once the OH group is no longer pointing in the direction of the acceptor oxygen atom, the H-bond is broken and the interaction between the donor and acceptor molecules becomes repulsive as seen from the negative slope of the potential surfaces in Figure 4. The dimer thus falls apart, and the torsion gradually releases more of its energy to the H-bond stretch. As mentioned earlier, this process is similar to the V−RT predissociation process of a variety of complexes that exhibit strong anisotropic interactions and large rotational constants for the excited fragment. Specifically for H-bonded complexes, it has been shown that the anisotropy of the H-bonding interaction turns a low-frequency rotational motion to a high-frequency interdimer bending motion, as in the case of the HF dimer.[28,32] When the vibration of the hydrogen-donating bond is excited, the interdimer bending motion absorbs the vibrational energy and the complex dissociates. We hypothesize that this pattern formed by the HF dimer, the HCl dimer,[49,50] and the methanol dimer might play an important role in H-bonding dynamics elsewhere. For example, it has been observed that the donor OH stretch region of the gas-phase water dimer consists of diffuse peaks, which have been attributed to lifetime broadening due to predissociation.[51]

While our results show that predissociation might be efficient enough to contribute to experimentally observed H-bond breaking, we cannot rule out the possible contribution from VER of the excited OH stretch. The time scale of VER of the OH stretch has been determined to be around 1 ps for neat methanol[34] and around 9 ps for monomeric methanol in CCl_4 solution.[52] The time scale for H-bonded methanol oligomers will most likely fall inside the 1−9 ps range. It is tempting to speculate that the predissociation and VER pathway both contribute to the H-bond breaking, a notion that is in line with Fayer and co-workers' results.[13−15] Furthermore, the strong dependence of predissociation lifetime on H-bond strength could potentially account for the preferential H-bond breaking reported by Fayer and co-workers.[16,17] However, more condensed-phase calculations are needed to quantify the time scales of the two competing pathways.

We now discuss the possibility of extending our calculation to the condensed phase. For instance, we can consider the system consisting of a methanol dimer immersed in CCl_4 solvents. It should be desirable to treat the solvent modes with classical

mechanics at relatively small computational cost while treating the intramolecular dimer modes faithfully with quantum mechanics. The H-bond stretch should receive a classical-like treatment since its motion is on a comparable time scale as the solvent modes. The SCF representation provides a convenient platform for such a mixed quantum−classical treatment. For every solvent configuration, SCF potentials similar to those in Figure 4 can be calculated with added solvent−solute interaction. The H-bond stretch can be thought of as a particle that starts off on the bound surface. As it evolves along the bound surface it will encounter crossings with various dissociative surfaces, where it has a certain probability of hopping onto the dissociative surfaces. Since these dissociative surfaces are mostly repulsive, the dimer will quickly dissociate. This curve crossing picture of predissociation has been proposed previously by Ewing[53] in the case of the C_2H_4 dimer. A variety of computational procedures including Landau−Zener, surface hopping,[54] and multiple spawning[55] are well suited for the treatment of this type of problem.

VI. Conclusion

We have constructed a four-dimensional model system for the methanol dimer. After some adjustment, the model reproduces the experimental vibrational frequencies reasonably well. A vibrational SCF representation, which is pseudodiabatic in essence, has been devised to carry out FGR calculations. This combination is found to be an efficient procedure for calculating lifetimes. The accuracy of the method has been demonstrated by comparing results with CC calculations.

Our results indicate that, the predissociation mechanism, where the OH stretch energy is solely transferred into the H-bond stretch, is highly inefficient. Instead, the OH stretch energy is transferred into the OH torsion and promotes over-the-barrier rotation of the OH group, which leads to H-bond breaking. This mechanism is similar to that of a series of H-bonded dimers and other weakly bound complexes. The common ground shared by these complexes is the anisotropic interaction between the two fragments and the small moment of inertia for the rotation around one axis of the excited fragment. These two conditions create a high-frequency intermolecular bending mode that can efficiently absorb the initially deposited energy. The predissociation rate is also found to strongly depend on the strength of the H-bond. For a dimer with H-bond strength typical of alcohol oligomers, predissociation occurs on a time scale of a few picoseconds. Meanwhile, the COH bend does not have a significant impact on the predissociation. We know that the COH bend is strongly mixed with other modes like the CO stretch. Moreover, there has been evidence that suggests the CO stretch is also strongly coupled to the OH torsion.[56] Thus it would be interesting to see how the results change when we include other intramolecular vibrations such as the CO stretch in future studies.

Although the above-mentioned mechanism is likely to play a role in the experimentally observed H-bond breaking, we cannot yet draw definitive conclusions without quantitative condensed-phased simulations. The curve crossing picture that emerges from our SCF representation provides a framework for the mixed quantum−classical simulation of the predissociation of a quantal solute complex in classical solvent. Future research along this line will help elucidate the experimental findings and improve our understanding of the dynamics of H-bonded liquids in general.

Acknowledgment. This material is based upon work supported by the National Science Foundation under Grant No. CHE-0615165.

References and Notes

(1) Ladanyi, B. M.; Skaf, M. S. *Annu. Rev. Phys. Chem.* **1993**, *44*, 335.
(2) Moller, K. B.; Rey, R.; Hynes, J. T. *J. Phys. Chem. A* **2004**, *108*, 1275.
(3) Lawrence, C. P.; Skinner, J. L. *J. Chem. Phys.* **2003**, *118*, 264.
(4) Eisenberg, D.; Kauzmann, W. *The Structure and Properties of Water*; Oxford University Press: New York, 1969.
(5) Nienhuys, H. K.; Woutersen, S.; van Santen, R. A.; Bakker, H. J. *J. Chem. Phys.* **1999**, *111*, 1494.
(6) Steinel, T.; Asbury, J. B.; Zheng, J. R.; Fayer, M. D. *J. Phys. Chem. A* **2004**, *108*, 10957.
(7) Wang, Z. H.; Pang, Y.; Dlott, D. D. *J. Phys. Chem. A* **2007**, *111*, 3196.
(8) Ashihara, S.; Huse, N.; Espagne, A.; Nibbering, E. T. J.; Elsaesser, T. *J. Phys. Chem. A* **2007**, *111*, 743.
(9) Graener, H.; Ye, T. Q.; Laubereau, A. *J. Chem. Phys.* **1989**, *90*, 3413.
(10) Laenen, R.; Rauscher, C. *J. Chem. Phys.* **1997**, *106*, 8974.
(11) Woutersen, S.; Emmerichs, U.; Bakker, H. J. *J. Chem. Phys.* **1997**, *107*, 1483.
(12) Laenen, R.; Gale, G. M.; Lascoux, N. *J. Phys. Chem. A* **1999**, *103*, 10708.
(13) Levinger, N. E.; Davis, P. H.; Fayer, M. D. *J. Chem. Phys.* **2001**, *115*, 9352.
(14) Gaffney, K. J.; Piletic, I. R.; Fayer, M. D. *J. Phys. Chem. A* **2002**, *106*, 9428.
(15) Gaffney, K. J.; Davis, P. H.; Piletic, I. R.; Levinger, N. E.; Fayer, M. A. *J. Phys. Chem. A* **2002**, *106*, 12012.
(16) Asbury, J. B.; Steinel, T.; Stromberg, C.; Gaffney, K. J.; Piletic, I. R.; Fayer, M. D. *J. Chem. Phys.* **2003**, *119*, 12981.
(17) Asbury, J. B.; Steinel, T.; Fayer, M. D. *J. Phys. Chem. B* **2004**, *108*, 6544.
(18) Miller., R. E. *Science* 1988, *240*, 447.
(19) Yamaguchi, T.; Hidaka, K.; Soper, A. K. *Mol. Phys.* **1999**, *97*, 603.
(20) Hoffbauer, M. A.; Giese, C. F.; Gentry, W. R. *J. Phys. Chem.* **1984**, *88*, 181.
(21) Buck, U.; Huisken, F. *Chem. Rev.* **2000**, *100*, 3863.
(22) Oxtoby, S. V. D. W. *J. Chem. Phys.* **1980**, *72*, 2260.
(23) Staib, A.; Hynes, J. T. *Chem. Phys. Lett.* **1993**, *204*, 197.
(24) Staib, A. *J. Chem. Phys.* **1998**, *108*, 4554.
(25) Kayano, M.; Ebata, T.; Yamada, Y.; Mikami, N. *J. Chem. Phys.* **2004**, *120*, 7410.
(26) Shipman, S. T.; Douglass, P. C.; Yoo, H. S.; Hinkle, C. E.; Mierzejewski, E. L.; Pate, B. H. *Phys. Chem. Chem. Phys.* **2007**, *9*, 4572.
(27) Rosen, N. *J. Chem. Phys.* **1933**, *1*, 319.
(28) Ewing, G. E. *J. Chem. Phys.* **1980**, *72*, 2096.
(29) Beswick, J. A.; Jortner, J. *J. Chem. Phys.* **1978**, *68*, 2277.
(30) Hutson, J. M.; Roy, R. J. L. *J. Chem. Phys.* **1983**, *78*, 4040.
(31) Hutson, J. M. *J. Chem. Phys.* **1984**, *81*, 2357.
(32) Halberstadt, N.; Brechignac, P.; Beswick, J. A.; Shapiro, M. *J. Chem. Phys.* **1986**, *84*, 170.
(33) Hutson, J. M.; Clary, D. C.; Beswick, J. A. *J. Chem. Phys.* **1984**, *81*, 4474.
(34) Iwaki, L. K.; Dlott, D. D. *J. Phys. Chem. A* **2000**, *104*, 9101.
(35) Gulmen, T. S.; Sibert, E. L. *J. Phys. Chem. A* **2005**, *109*, 5777.
(36) Wilson, E. B.; Decius, J. C.; Cross, P. C. *Molecular Vibrations: The Theory of Infrared and Raman Vibrational Spectra*; Courier Dover Publications: New York, 1980.
(37) Frisch, M. J.; Trucks, G. W.; Schlegel, H. B.; Scuseria, G. E.; Robb, M. A.; Cheeseman, J. R.; Zakrzewski, V. G.; Montgomery, J. A., Jr.; Stratmann, R. E.; Burant, J. C.; Dapprich, S.; Millam, J. M.; Daniels, A. D.; Kudin, K. N.; Strain, M. C.; Farkas, O.; Tomasi, J.; Barone, V.; Cossi, M.; Cammi, R.; Mennucci, B.; Pomelli, C.; Adamo, C.; Clifford, S.; Ochterski, J.; Petersson, G. A.; Ayala, P. Y.; Cui, Q.; Morokuma, K.; Salvador, P.; Dannenberg, J. J.; Malick, D. K.; Rabuck, A. D.; Raghavachari, K.; Foresman, J. B.; Cioslowski, J.; Ortiz, J. V.; Baboul, A. G.; Stefanov, B. B.; Liu, G.; Liashenko, A.; Piskorz, P.; Komaromi, I.; Gomperts, R.; Martin, R. L.; Fox, D. J.; Keith, T.; Al-Laham, M. A.; Peng, C. Y.; Nanayakkara, A.; Challacombe, M.; Gill, P. M. W.; Johnson, B.; Chen, W.; Wong, M. W.; Andres, J. L.; Gonzalez, C.; Gordon, M. H.; Replogle, E. S.; Pople, J. A. *Gaussian 98*, Revision A.1x; Gaussian Inc.: Pittsburgh, PA, 2001.
(38) Bowman, J. M. *Acc. Chem. Res.* **1986**, *19*, 202.
(39) Gerber, R. B.; Ratner, M. A. *Chem. Phys. Lett.* **1979**, *68*, 195.
(40) Gerber, R. B.; Ratner, M. A. *Adv. Chem. Phys.* **1988**, *70*, 97.
(41) Atchity, G. J.; Ruedenberg, K. *Theor. Chem. Acc.* **1997**, *97*, 47.
(42) Nakamura, H.; Truhlar, D. G. *J. Chem. Phys.* **2001**, *115*, 10353.

(43) Colbert, D. T.; Miller, W. H. *J. Chem. Phys.* **1992**, *96*, 1982.
(44) Levine, I. N. *Quantum Chemistry*; Prentice Hall: Upper Saddle River, NJ,1991.
(45) Schinke, R. *Photodissociation dynamics: spectroscopy and fragmentation of small polyatomic molecules*; Cambridge University Press: New York, 1995.
(46) Stechel, E. B.; Walker, R. B.; Light, J. C. *J. Chem. Phys.* **1978**, *69*, 3518.
(47) Ashton, C. J.; Child, M. S.; Hutson, J. M. *J. Chem. Phys.* **1983**, *78*, 4025.
(48) Hunt, R. H.; Shelton, W. N.; Flaherty, F. A.; Cook, W. B. *J. Mol. Spectrosc.* **1998**, *192*, 277.
(49) Serafin, J.; Ni, H.; Valentini, J. J. *J. Chem. Phys.* **1994**, *100*, 2385.
(50) Vissers, G. W. M.; Oudejans, L.; Miller, R. E.; Groenenboom, G. C.; van der Avoird, A. *J. Chem. Phys.* **2004**, *120*, 9487.
(51) Huang, Z. S.; Miller, R. E. *J. Chem. Phys.* **1989**, *91*, 6613.
(52) Laenen, R.; Simeonidis, K. *Chem. Phys. Lett.* **1999**, *299*, 589.
(53) Ewing, G. E. *Chem. Phys.* **1981**, *63*, 411.
(54) Tully, J. C. *J. Chem. Phys.* **1990**, *93*, 1061.
(55) Ben-Nun, M.; Quenneville, J.; Martinez, T. J. *J. Phys. Chem. A* **2000**, *104*, 5161.
(56) van den Broek, M. A. F. H.; Nienhuys, H. K.; Bakker, H. J. *J. Chem. Phys.* **2001**, *114*, 3182.
(57) Larsen, R. W.; Zielke, P.; Suhm, M. A. *J. Chem. Phys.* **2007**, *126*, 194307.
(58) Serrallach, A.; Meyer, R. G. *J. Mol. Spectrosc.* **1974**, *52*, 94.
(59) Burkhard, D. G.; Dennison, D. M. *J. Mol. Spectrosc.* **1959**, *3*, 299.
(60) Larsen, R. W.; Suhm, M. A. *J. Chem. Phys.* **2006**, *125*, 154314.

JP8104776